Revised: July 12, 2002

Tests of Potential Energy Surfaces for $H + CH_4 \leftrightarrow CH_3 + H_2$: Deuterium and Muonium Kinetic Isotope Effects for the Forward and Reverse Reaction

Jingzhi Pu and Donald G. Truhlar
Department of Chemistry and Supercomputer Institute, University of Minnesota, 207 Pleasant Street S.E., Minneapolis, MN 55455-0431

Abstract. In previous work, three implicit potential energy surfaces (PESs) with specific reaction parameters (SRP), namely MPW60, MC-QCISD-SRP, and MCG3-SRP, were developed for the reaction $CH_4 + H \rightarrow CH_3 + H_2$. Forward reaction rate constants obtained by variational transition state theory with multidimensional tunneling (VTST/MT) dynamics calculations on these surfaces give good agreement with recently re-analyzed experimental results. In the present work, again employing VTST/MT, kinetic isotope effects (KIEs) for isotopic variants of the title reaction in both the forward and reverse directions are examined on these SRP surfaces. Various primary and secondary deuterium (D) kinetic isotope reactions are studied; we also calculated the KIE for the reaction between methane and muonium (Mu), which is an ultralight isotope of protium with the Mu/H mass ratio being 0.113. The results are compared with several sets of experimental studies. With the VTST/MT dynamical method and harmonic vibrations, the proposed surfaces predict the KIE quite well, probably within experimental error, for seven different isotopic combinations involving substitution of one to five deuteriums for protium. The calculations also reproduce quite well the high Arrhenius activation energy for $Mu + CH_4$, and the KIE for muonium atom attack is correctly predicted to be inverse, but the predicted values of the Um KIE over the experimental temperature range are 0.012 – 0.06 (without scaling force constants) or 0.021 – 0.09 (when the force constant of the making bond is scaled), whereas the experimental values in the same temperature range are 0.05 – 0.3. Several possible reasons for this are discussed.

I. INTRODUCTION

We have recently proposed three new implicit potential energy surfaces (PESs) with specific-reaction parameters (SRP) for the reaction:

$$H + CH_4 \rightarrow H_2 + CH_3 \qquad R1$$

and its reverse.[1] The first SRP PES is called MPW60; it is based on modified Perdew-Wang (mPW) hybrid density functional theory[2] with the percentage of Hartree-Fock (HF) exchange adjusted to 60%. The other two PESs, i.e., MC-QCISD-SRP and MCG3-SRP, were constructed from multi-coefficient correlation methods (MCCMs).[3-7] All three SRP surfaces have a classical barrier height of 14.8 kcal/mol. The two MCCM surfaces also reproduce the experimental reaction endoergicity of 3.3 kcal/mol. We have shown that dynamics calculations carried out on the MPW60 surface and the two MCCM surfaces can reproduce the recently re-analyzed experimental rate constants[8] for the reaction (1) over a wide temperature region from 348 K to 1950 K.[1]

In the present paper we test these surfaces by using them to predict kinetic isotope effects (KIEs) for isotopic variants of reaction (1) involving deuterated methane, deuterium, and muonium atom. Due to the large mass ratios among various isotopes of hydrogen, reaction rates of hydrogenic isotopes can be very different from one another.[9] One can ascribe this effect primarily to changes of the effective tunneling mass, quantized vibrational energy, and moments of inertia. The change in the vibrational zero point energy (ZPE) along the reaction coordinate, leads to a change in the shape and width of the effective barrier, resulting in an isotope-dependent location of the variational transition state and contributing a multi-dimensional aspect to the tunneling probability. Because dynamics calculations are carried out on the same Born-Oppenheimer potential energy surface for all isotopic reactions, KIEs provide challenging tests of the accuracy of potential energy surfaces and the validity of dynamical theories.

Hydrogen has three well-known isotopes, protium(H), deuterium(D), and tritium(T), and predicting reaction rates as a function of isotopic substitution is an important testing

ground for theory . In addition, hydrogen has a fourth (nonconventional) isotope, which provides an even more demanding test of theory.[10] Muonium is composed of a muon (μ^+) and an electron and can be treated as an ultralight hydrogenic isotope compared to protium because the muon possesses only one-ninth of the mass of a proton. Due to quantum tunneling effects and large differences in the quantized vibrational energies, processes involving Mu can exhibit very different dynamical properties than the reactions of other isotopes of hydrogen.[10-24]

With the development of the muon spin rotation (μSR) technique,[10] reaction rates of Mu can be measured accurately. For example, experiments have been carried out for the reactions of Mu with with N_2O,[11] O_2,[12] H_2 and D_2,[13] halogens,[14] CH_4,[15] and C_2H_6.[15,16] Interestingly, the reaction of Mu with methane ($Mu + CH_4 \rightarrow MuH + CH_3$) has an activation energy E_a of 20 – 26 kcal/mol over the temperature range 625 – 820 K (computed from the rate constants of Ref. 15), which is about 7 – 13 kcal/mol higher than that of the H-atom isotopic variant of this reaction. This E_a difference between H and Mu is the largest yet seen at high temperatures in the gas phase. A simple comparison of estimated zero-point-energy (ZPE) difference at the respective saddle points of H and Mu reactions is insufficient to explain and to explain this dramatic isotope effect. More careful theoretical calculations are necessary for interpretation of the experimental results.

In the present paper, we report direct dynamics calculations[25] carried out on implicit *ab initio* potential energy surfaces parameterized[1] for the title reaction. We employ canonical variational transition-state-theory (CVT)[26,27] with multidimensional tunneling (MT). The MT calculations include the small-curvature tunneling approximation (SCT),[28,29] the large-curvature tunneling approximation (LCT),[29-31] and the microcanonically optimized mulitidimensional tunneling approximation (μOMT).[32] This dynamical model is used to investigate KIEs for reaction R1 involving deuterated methane, deuterium atom, and muonium atom. These calculations not only test the

validity of the implicit PESs, but also they provide us important information on the dynamical behavior of an ultralight atom in a polyatomic reaction. Conventional transition state theory calculations have been carried out by Schatz *et al*.[33] for many of the same isotopic combinations as we considered in this paper, and we refer the reader to their paper for a comparison.

In Section II we summarize the potential energy surfaces that are used in the present study. In Section III, we present the computational details of the present dynamics calculations, including a new method for scaling principal force constants in internal coordinates. In Section IV we present the results and compare the calculated reaction rates to experimental values. Sections V and VI contain results and discussion and concluding remarks.

II. POTENTIAL ENERGY SURFACES

The parameterization and stationary points of the three SRP potential energy surfaces have been described in detail in our previous work.[1] Here we present a brief summary.

The first SRP approach we used is called MPW*X*; it is based on the mPW hybrid density functional method[2] with the percentage *X* of HF exchange being parameterized for a specific reaction to obtain agreement with experimental kinetic data. Previously, we have presented version of MPW*X* with general parameters. This is called MPW1K, and it has been shown to be an especially powerful way to obtain potential energy data for kinetics calculations.[34] In MPW1K, the percentage of HF exchange was optimized to 42.8% by fitting to barrier heights and reaction energies of 20 chemical reactions.[34] Our direct dynamics studies of the prototype reaction R1 showed that an increase of the HF exchange to 60% is necessary for one to obtain a barrier height of 14.8 kcal/mol, which is our best estimate on the basis of comparing a variety of dynamics calculations to the experimental rate constants of reaction R1 from 348 to 1950 K. However, the stationary-

point frequencies were found to be overestimated at the MPW60 level. We will investigate the sensitivity of the KIEs to this difficulty in the present study.

The other two implicit SRP surfaces that we test in the present study are based on recently developed multi-coefficient correlation methods (MCCMs).[3-7] MCCMs are designed to extrapolate electronic structure calculations to include the effects of full configuration interactions and an infinite basis set by combining several single-level calculations. We parametrized two of most accurate MCCMs, in particular, MC-QCISD and MCG3, for the specific reaction of H with CH_4 by varying the two most sensitive multilevel coefficients in the set of global or semiglobal parameters. The final MCCM surfaces with specific reaction parameters are labeled with the suffix "-SRP" to differentiate them from the versions based on global or semiglobal parameters.

All three of these SRP surfaces, i.e., MPW60, MC-QCISD-SRP, and MCG3-SRP, have an empirical zero-point-exclusive barrier height of 14.8 kcal/mol. Because we were able to vary more than one parameters during the parametrizations of MC-QCISD-SRP and MCG3-SRP, we also adjusted[1] these two MCCM surfaces to reproduce our best estimate[1] of the zero-point-exclusive endoergicity of title reaction, 3.3 kcal/mol.

Details of the stationary-point properties of these SRP surfaces including geometries of the saddle point and normal mode frequencies and vibrational ZPEs of reactants, saddle point, and products can be found in our previous paper.[1]

III. DYNAMICS CALCULATIONS

III. A. Dynamics with harmonic vibrations

The atomic masses for H, D, and Mu used in the present calculations are 1.0078, 2.0140, and 0.1140 amu respectively.

The scaling mass[29] for all coordinates is set equal to 1 amu; this affects the numerical values of the reaction coordinate *s*, and the step sizes, but has no effect on predicted observables. The minimum energy path (MEP) in isoinertial coordinates is

calculated by the Euler steepest-descent method combined with the reorientation of the dividing surface (ESD/RODS) algorithm[35] with a gradient step size of 0.01 a_0 and with the Hessian being calculated every 9 steps. In the present study, a converged reaction path is calculated from −1.5 a_0 on the reactants side to +1.5 a_0 on the product side. The generalized normal mode analysis at Hessian points along the reaction path is implemented using a set of redundant curvilinear internal coordinates.[36] (The vibrational frequencies for reactants and products are also calculated in internal coordinates, which are obtained by splitting the whole set of redundant curvilinear internal coordinates into corresponding sub-sets applicable to each species; however, at stationary points one would obtain the same frequencies with rectilinear coordinates.) The reaction rate constants are calculated using canonical variational transition-state-theory (CVT)[26,27] with multidimensional tunneling in the small-curvature tunneling (SCT),[28,29] large-curvature tunneling (LCT),[29-31] and microcanonically optimized multidimensional tunneling (μOMT)[31,32] approximations. The details of CVT/SCT, CVT/LCT, and CVT/μOMT calculations can be found elsewhere;[26-31,37] all LCT and μOMT calculations are based on the version-4 algorithm[31] and are converged with respect to the number of excited states. All geometry optimizations[38] and dynamics calculations[26-31,37] on multi-level implicit potential energy surfaces are done using the computer program MULTILEVELRATE,[39] which interfaces the VTST/multidimensional-tunneling program POLYRATE[29,40] to the electronic structure program MULTILEVEL.[41] The calculations on MPW*X* surfaces are carried out using GAUSSRATE.[42] All electronic structure calculations are carried out with GAUSSIAN98.[43]

III. B. Scaling internal force constants

Calculations of KIEs are particularly sensitive to employing accurate values for quantized vibrational energies, and this sensitivity is exacerbated for systems involving Mu because the ZPE of stretching modes involving Mu is very large. A small percentage

error in the ZPE of a mode with large Mu-H stretching character can correspond to an appreciable error in energy units and hence can have a large effect on rate constants. Errors in the ZPE of stretching modes arise from two sources: inaccuracies in the potential energy surface and neglect of anharmonicity. We have developed a simple force constant scaling procedure that can reduce the error coming from both of these sources. The method is very simple and it is very general in that it may be used for arbitrary KIE calculations involving deuterium or any other isotope of interest; however we illustrate it here by applying in terms of the Mu-H bond formed in reaction R6 (see Table 1) and the corresponding H-H bond formed in reaction R1.

The energy levels of a Morse oscillator are[44]

$$\varepsilon(n) = \frac{1}{2}\hbar\omega_e(n+\frac{1}{2})[1 - x_e(n+\frac{1}{2})] \qquad (1)$$

where n is the vibrational quantum number, ω_e is the harmonic vibrational frequency, x_e is the anharmonicity constant given by

$$x_e = \hbar\omega_e / 4D_e \qquad (2)$$

and is D_e is the equilibrium dissociation energy. The ZPE with anharmonicitity included can be expressed as:

$$\mathrm{ZPE} = \frac{1}{2}\hbar\omega_e(1-\frac{x_e}{2}) = (1-\frac{x_e}{2})\mathrm{ZPE_{HO}} \qquad (3)$$

where a subscript HO denotes the value for the corresponding harmonic oscillator. The goal is to scale the stretching force constant so that a dynamics calculation with the harmonic approximation will mimic an anharmonic calculation for a given isotopic combination and will also mimic the use of a more accurate force constant. Thus, the effective force constant is expressed as:

$$f = (1-\frac{x_e}{2})^2 f_{\mathrm{HO}} = (\frac{\mathrm{ZPE}}{\mathrm{ZPE_{HO}}})^2 f_{\mathrm{HO}} \qquad (4)$$

where f and f_{HO} are the effective force constant and harmonic force constant respectively. We assume that x_e is constant along the reaction path. Then the effective force constant for the stretch vibration of the making bond stretch can be then computed from eq. (4),

where f_{HO} is the value obtained by Taylor series of the potential along the reaction path. At each point along the reaction path we then substitute this scaled f for f_{HO} in the vibrational analysis of Refs. 36 and 37.

IV. RESULTS

The isotopic reactions we investigate in the present study are listed in Table 1 with the corresponding reaction symmetry factors σ. (Note that the symmetry numbers for the reverse reaction correctly assume planar CH_3.) In the present work the KIE is defined as the ratio k_i/k_j, where k_i represents the rate constant for the isotopic reaction with lighter mass, and k_j represents the rate constant for the corresponding heavier isotopic reaction. In the case of the KIE for R4 vs. R5 or R9 vs. R10, we put the R4 and R9 rate constants in the numerator because they have a smaller mass for the transferred atom.

Tables 2 to 7 show the kinetic isotope effects (KIEs) for reactions involving deuterated methane and deuterium at various levels of dynamical theory, i.e., conventional transition state theory (TST), canonical variational transition-state-theory (CVT), and canonical variational transition state theory with multidimensional tunneling calculated by small-curvature (CVT/SCT) tunneling, by large-curvature tunneling (CVT/LCT), and by the microcanonically optimized multidimensional tunneling approximation (CVT/μOMT). For reactions in Tables 2 and 3, we compare to experimental KIEs[45] used by Espinosa-García and Corchado for comparison to their earlier theoretical studies.[46] For reactions in Tables 4 and 5, we compare to experimental KIEs[45a,47] used by Truhlar *et al*. in an earlier analysis.[9b] The experimental KIE values for comparison in Table 6 and Table 7 are obtained from measurements of Shapiro and Weston.[45a] In Table 8, we obtained the experimental KIE directly using rate constants measured by Kurylo *et al*.[48] for both isotopic reactions involved in each KIE. In Table 9, the experimental KIEs are from the pairs in Tables 2 and 5; results from pairs in Tables 4 and 7 are also given for comparison.

To elucidate KIEs for reactions involving Mu, we list isotopic rate constants as well as the KIEs at each temperature. Table 10 presents the calculated reaction rate constants for Mu + CH_4 and compares them with experimental rate constants[15] at the temperatures of the actual experiments. The calculated reaction rate constants of the prototype reaction R1 are listed in Table 11 where they are compared with the latest re-analyzed[8] experiment results; we note that this re-analysis was shown[8a] to be able to resolve previous inconsistencies that impeded testing of new PESs for reaction R1. In Table 12, we present the KIEs for the reaction Mu + CH_4.

The Arrhenius activation energy, defined by

$$E_a = -R \frac{d \ln k}{d (1/T)} \qquad (5)$$

is a fundamental quantity in chemical kinetics in that it characterizes the difference between the average energy of reacting pairs of reagents and the average energy of all pairs.[49] The Arrhenius activation energy, also known as the phenomenological activation energy, is well known to depend on temperature and isotopic composition.[20,50] Its value at any given temperature can be evaluated by a finite difference approximation of the derivative in eq. (5) or by analytic differentiation of a fit to temperature dependence of $k(T)$. Using the data in Tables 2 – 12 and additional data in the references of these tables, we can evaluate experimental values of E_a for six of the ten reactions in this paper at 650 K. We give these values along with theoretical values for the same six reactions in Table 13.

Table 14 shows the values of key geometrical and energetic quantities for two of the implicit potential energy surfaces for reactions R6, R1, and R3, where we increase the mass of the attacking atom from ~1/9 to ~1 to ~2. In particular, these quantities are compared at the saddle point and at the variational transition state locations at three different temperatures. The quantities compared are the value s of the reaction coordinate, the values $r_{C\text{-}H}$ and $r_{H\text{-}Y}$ of the breaking and making bond distances,

respectively, the value V_{MEP} of the potential energy along the MEP, the harmonic zero point energy, and the vibrationally adiabatic ground-state potential defined by

$$V_a^G(s) = V_{MEP}(s) + ZPE(s) \quad (6)$$

All quantities in Table 2 – 14 were calculated with the harmonic approximation for vibration with the implicit potential energy surfaces developed in Ref. 1. Although the harmonic approximation can lead to systematic errors for the partition function of the reactants or a generalized transition state, we have found that these errors largely cancel one another in the calculation of rate constants, at least for atoms as heavy as protium.[51,52] However, as mentioned in Section III.B, the effects of anharmonicity and inaccurate harmonic force constants may be unusually large in reactions forming Mu-H bonds, and we developed a method for scaling a principal stretching force constant in internal coordinates to reduce these errors. In the current work, we scale only one force constant, namely that for the making bond, because this internal coordinate (since it has the smallest reduced mass of any stretch and the largest inaccuracy in force constant along the reaction path) is expected to have the largest anharmonicity contribution to the change in zero point energy along the reaction path when we quantize the vibrational modes of reaction R6. For consistency in the KIE calculations, the same scaling strategy is applied to the H-H stretch of the making bond in the unsubstituted CH_4 + H reaction, reaction R1.

To illustrate the sensitivity to including zero point energy, we will give results obtained with scaled force constants for the MPW60 and the MCG3-SRP surfaces. On the MPW60 surface, the harmonic zero point energy of H_2 is 6.5615 kcal/mol, whereas the correct anharmonic value should be 6.21 kcal/mol;[53] therefore the force constant scaling factor $(f/f_{HO})_{H\text{-}H}$ and the effective anharmonicity constant $(x_e)_{H\text{-}H}$ for the H-H stretching are calculated as 0.8957 and 0.1071 respectively using eq. (4). The corresponding anharmonicity constant for H-Mu stretching $(x_e)_{H\text{-}Mu}$ can be obtained by[44]

$$(x_e)_{\text{H-Mu}} = \sqrt{\frac{\mu_{H_2}}{\mu_{HMu}}}\,(x_e)_{\text{H-H}} \qquad (7)$$

as 0.2376, resulting in a force constant scaling factor $(f/f_{HO})_{\text{H-Mu}}$ of 0.7765 [from eq. (4)] for the H-Mu stretching force constant. Thus, we scale the making-bond force constants by different scaling factors for each isotopic combination to simulate the isotope-dependent zero point energy more accurately. The force constant scaling factors for H-H and H-Mu stretching on the MCG3-SRP surface can be obtained in the same way as 0.9746 and 0.9441, respectively. Notice that the scaling treatment corrects a significant systematic error in the MPW60 harmonic force constant as well as accounting for anharmonicity, whereas in the MCG3-SRP case it mainly account for anharmonicity. For consistency, we systematically scale the stretching force constant for the making bond all along the reaction path, i.e., for saddle point, products, and generalized transition state points along the MEP. The total zero point energies without and with scaling the force constants for the making bond are given in Table 15. The rate constants and KIEs (CH_4 +Mu/CH_4+H) obtained with scaling are shown in Tables 16 and 17 and in Fig. 1. The vibrationally adiabatic ground-state potential energy curves for these two cases are shown in Fig. 2, and the profiles of the individual normal mode frequencies are shown in Fig. 3.

Table 18 compares the predicted geometries for the methyl radical to experiment[54] and shows good agreement.

Table 19 gives absolute rate constants at 600 K and 700 K for all reactions since these can not all be computed from the ratios in earlier tables.

V. DISSCUSSION

The final calculated values are obtained by the CVT/μOMT method; all other results (TST, CVT, CVT/SCT, and CVT/LCT) are given only for comparison of trends. All of the final calculated KIEs that involve only deuterium and protium reproduce the

experimental result very successfully. Considering all seven of these KIEs, the MPW60 and MCG3-SRP surface seem to perform slightly better than MC-QCISD-SRP, and they may well agree with experiment within the experimental reliability in all cases; it is difficult to assess the potential systematic errors in the experimental values because most of the experimental rate constants have been measured only once. For more detailed analysis we concentrate on the MCG3-SRP surface and the CVT/μOMT dynamical method since *a priori* that should be our best calculation. (However, the MPW60 case is also of special interest because it is the least expensive option for future direct dynamics calculations.) For six of the seven deuterium KIEs, the combination of MCG3-SRP and CVT/μOMT appears to agree with experiment within the experimental reliability at all temperatures (although the disagreement is most serious for $CH_3/CD_3 + D_2$ at 400 – 500 K in Table 5); and for the other case, H_2/D_2 with CD_3 (Table 7), the predictions clearly agree with experiment within experimental errors at 500 – 700 K, but the predicted KIEs are 24% high at 400 K. On the whole, the agreement of theory and experiment is quite gratifying, although further work on the cases in Tables 5 and 7 would be interesting. We do not know the source of the large disagreement in these two cases, and it would be worthwhile to check both the experiment and the theory.

The predictions of the isotope-dependent activation energies at 650 K (Table 13) agree with experiment for reactions R1 – R3, R7, and R8 within errors of 0.6 kcal/mol, which may well be smaller than the experimental uncertainties. It is very encouraging that the theoretical calculations agree *perfectly* with experiment for the order of the activation energies: $CH_4 + Mu > CH_4 + H > CH_4 + D > CD_3 + D_2 > CH_3 + H_2 > CD_3 + H_2$. Furthermore, even at this reasonably high temperature (650 K), the CVT/μOMT calculations agree with experiment much better than the conventional TST or CVT ones without tunneling. In the Mu case, even though the Arrhenius fit[15] of the rate constants over the whole experimental temperature range gave an activation energy of 24.6 kcal/mol,[15] finite differentiation of the actual experimental rate constants at 634 K and

668 K results in an activation energy of only 20.6 kcal/mol, in good agreement with our calculations. The activation energy obtained as the local Arrhenius slope of the smoothed temperature-dependent data increases from about 20 to 26 kcal/mol over the experimental temperature range. Some further discussion of the experimental temperature dependence in the Mu case may be warranted. First of all, the experimentalists noted[15] that the temperature of the highest temperature point may be as much as 14 K higher than the nominal 821 K that they assigned it, although for temperatures of 626 – 691 K with smaller errors of 2 – 5 K for 721 – 776 K, the nominal temperature should be reliable within 1 K or better. They estimated that this temperatures-dependent systematic error could lead to a systematic overestimate of the experimental energy of activation. We find that it decreases the local slope at high T from about 26 kcal/mol to about 24 kcal/mol. The point of including more than one value of E_a for this reaction in Table 13 is not to argue that any one of these values is accurate to better than 1 kcal/mol but rather to show that there is uncertainty in the experimental values.

In the reaction of methane with atomic Mu, the reaction rate constants calculated without scaling are too small compared to experimental values, resulting in an underestimate of the KIEs by factors of 3 – 6 (if we use Ref. 8a) or 3 – 5 (if we use Ref. 8b) in the temperature region we investigate. There might be several reasons for this poor prediction of the rate constants in the Mu case:

(1) Mu is an ultralight isotope of H with a mass only one-ninth of that for H. One might question whether the Born-Oppenheimer approximation is still valid for all reactions involving Mu, although previous work on Mu KIEs has not required invoking Born-Oppenheimer breakdown.[19, 23, 24, 55] Based on scaling the results for protium reactions,[56] this seems unlikely to be the major source of error (a factor 2), but it may be quantitatively important.

(2) Mu KIEs provide a strict test of the global validity of the potential energy surface. Comparing the KIEs at the TST level with KIEs at the CVT level, we find

variational effects (defined as the differences of CVT from TST) on the KIEs of non-Mu reactions of no more than 21% (see Tables 2 – 9) whereas Table 12 shows variational effects of 33 – 50% for Mu. Table 16 shows effects up to 62%, and Table 17 shows effects up to 69%. These pronounced variational effects for Mu are due to very significant change in vibrational frequencies along the reaction path (see Fig. 3). Thus, even though the PESs we proposed are fitted to experimental data, the fit mainly adjusts the classical barrier height near the dynamical bottleneck for R1, but the dynamical bottleneck for R6 is significantly later (see Fig. 2); in fact, if the position of the bottleneck of reaction R6 is far from the saddle point, that may deteriorate the usefulness of our parametrization of the PESs. The variational effect on the dynamic bottleneck for various isotopic reactions on the MPW60 and the MCG3-SRP surfaces is illustrated in Table 14. At the variational transition state for 600 K, the breaking bond in the Mu reaction is ~0.05 Å longer than the breaking bond in the H or D atom reactions, and the corresponding making bond length is ~0.01 Å shorter, indicating a late transition state in CH_4 + Mu. Since the effect is < 0.1 Å, this is probably not the major source of error.

(3) Since we obtain good agreement with experimental rate constants for H + CH_4, but we an apparently underestimate the rate of Mu + CH_4, we cannot discount the possibility of the experimental error in the Mu case, but it does seem unlikely that any experimental error would be large enough to fully accommodate the theoretical predictions.

(4) Extensive experience has indicated that semiclassical tunneling approximations, even in one dimension, can have intrinsic errors on the order of 10 – 15% as compared to full quantum mechanics for realistic barrier shapes and for reduced masses corresponding to hydrogenic movement in the reaction coordinate.[57] Participation of Mu lowers the effective reduced mass and raises the possible error in semiclassical methods. Our current best estimated (from Table 17) is that quantum effects on the reaction coordinate increases the reaction rate by factors of 2.6, 1.3, and 1.1 at 400, 626, and 821 K,

respectively, as compared to factors of 3.5, 1.6, and 1.3 respectively for R1 at these same three temperatures. One possibility is that the shape (especially the width) of the barrier is inaccurate in such a way that it decreases the tunneling for Mu more than for H. That seems unlikely to be the major source of error for two reasons. First, a major advantage of direct dynamics calculations with high-level electronic structure theory (such as MCG3-SRP) is that the barrier shape should be much more reliable than in old-fashioned calculations with analytically fitted potentials. Second, the error in our calculations increases with increasing temperature.

(5) The inclusion of a very accurate zero point energy is more important for the H-Mu stretch mode than that for an H-H stretch due to the large vibrational ZPE in a bond involving Mu. In fact, Tables 16 and 17 show the scaled-force-constant treatment does account for a significant part of the error at 626 K, especially for the MPW60 surface, but it has a much smaller effect at 821 K. It is especially encouraging that the use of scaled force constants for the making bond greatly reduces the deviation between the MPW60 and MCG3-SRP predictions for the Mu reaction; for example, at 626 K, a 43% deviation in Table 10 is reduced to 15% in Tables 16 and 17. Nevertheless it would be interesting to carry out a full calculation including anharmonicity more completely in bends as well as the stretching coordinate of the making bond and also including vibration-rotation coupling more completely. These are the chief areas where we expect the present calculation to be deficient.

(6) The possible experimental overheating effect mentioned above could lead to an overestimate of about 15% in the Mu + CH_4 rate constant at 776 – 821 K (from Fig. 1 of Ref. 15). This would lower the experimented KIEs from 0.18 – 0.22 to 0.16 – 0.19 at 776 K and from 0.27 – 0.32 to 0.24 – 0.28 at 821 K, which does improve the agreement with theory but not enough to remove the discrepancy.

Next we discuss some points of interpretation of the Mu + CH_4 that were raised by the experimentalists in Ref. 15 and by the referee. First of all, they suggested that the

energy of activation for R6 should exceed that for R1 by "at most" the ZPE difference between MuH and HH products. Such an argument neglects the ZPE of the Mu-H-C bend, the thermal excitation effects of vibrations and rotations, the isotopic dependence of variational effects, and tunneling. Second, they stated that the deviation of the experimental results from this kind of expectation indicates a qualitative difference "in the dynamics of Mu- and H- reactivity with methane" or "arises from differences in the effects of excited vibrational states on the dynamics". We prefer to avoid this kind of language, which in our opinion - is often based on a misunderstanding of transition state theory. Transition state theory corresponds to calculating the one-way dynamical flux through a phase space hypersurface separating reactants from products. It includes the dynamics of all excited vibrational states as well as the ground state, and it includes "dynamics" more accurately than many models that center attention on details of the dynamics that may be irrelevant for the net flux through the dynamical bottleneck but do not quantitatively include the quantum effects and the average over a canonical ensemble as fully as generalized transition state theory does. Thus we do not regard the difference between generalized-transition-state-theory and experiment as a measure of "dynamics". More often it indicates a deficiency in the potential energy surface, the quantitative treatment of anharmonicity or tunneling, the definition of the reaction coordinate, the neglect of a recrossing correction, or - more likely - more than one of these quantitative factors.

The experimentalists for then attempted to infer that excited states of methane are more reactive toward Mu than they are toward H and further to relate this to the isotopic dependence relative speed distributions, the isotopic dependence of noncollinear reaction paths, and the isotopic dependence of vibrational nonoadiabaticity. They even raised the issue of nonequilibrium effects. In general thermally averaged rate data is insufficient to extract such details of the dynamics because the details are masked out by the thermal averaging. Because systems with quite different state-to-state dynamics may have

essentially identical thermally averaged rate coefficients, attempts to extract such details from thermally averaged rate data in the absence of state-selected rate data, state-dependent molecular beam data, or state-dependent spectroscopic probe, is necessarily speculative and beyond the scope of the present study.

Generalized transition state theory does, however, lead to insight into the factors controlling the rate constant and activation energies. For example, comparing the CVT/SCT and CVT/LCT columns in Table 19 gives insight into the native of the tunneling process.[58] Furthermore, we can also understand in general way the isotope dependence of the activation energies.

VI. CONCLUDING REMARKS

In this work, we apply canonical variational transition-state-theory with multi-dimensional tunneling to test three implicit potential energy surfaces with specific reaction parameters (SRP) that were developed in our previous study for reaction R1. Kinetic isotope effects (KIEs) for various isotopic version of the reaction $CH_4 + H \leftrightarrow CH_3 + H_2$ involving deuterated methane, deuterium, and muounium atom are investigated. The calculated KIEs agree well with experimental results for reactions involving hydrogen and deuterium, although it would be worthwhile to check both the experiments and the theory for two of the cases. However, for KIEs of Mu reacting with methane, the calculations disagree with experiments based on the recommended rate constants for the $H + CH_4$ reaction by factors of 3 – 6 with unscaled direct dynamics and factors of 1.9 – 4.4 (MCG3-SRP) or 1.5 – 3.6 (MPW60) when the force constant for the making bond is scaled to reproduce the accurate zero point energy of H_2. The disagreements are slightly smaller, factors of 3 – 5, 1.8 – 3.8, and 1.5 – 3.0, respectively, if we accept the extrapolations of Ref. 8b instead of recommended value of Ref. 8a for the $H + CH_4$. We interpret the good prediction of H and D KIEs as confirmation of the

PESs, and we attribute the disagreement with experiment for Mu case as evidence for higher-order quantum effects, unusually large anharmonicity effects, or both.

ACKNOWLEDGMENTS

This work was supported in part by the U.S. Department of Energy, Office of Basic Energy Sciences.

References:

[1]J. Pu and D. G. Truhlar, J. Chem. Phys. **116**, 1468 (2002).

[2]C. Adamo and V. Barone, J. Chem. Phys. **108**, 664 (1998).

[3]P. L. Fast and D. G. Truhlar, J. Phys. Chem. A **104**, 6111 (2000).

[4]P. L. Fast, J. C. Corchado, M. L. Sánchez, and D. G. Truhlar, J. Phys. Chem. A **103**, 5129 (1999).

[5]C. M. Tratz, P. L. Fast, and D. G. Truhlar, PhysChemComm. **2**/**14**, 1 (1999).

[6]P. L. Fast, M. L. Sánchez, and D. G. Truhlar, Chem. Phys. Lett. **306**, 407 (1999).

[7]J. M. Rodgers, P. L. Fast, and D. G. Truhlar, J. Chem. Phys. **112**, 3141 (2000).

[8](a) J. W. Sutherland, M.-C. Su, and J. V. Michael, Int. J. Chem. Kinet. **33**, 669 (2001). (b) M. G. Bryukv, I. R. Slagle, and V. D. Knyazev, J. Phys. Chem. A **105**, 3107 (2001).

[9](a) W. H. Saunders, Jr., in *Investigation of Rates and Mechanisms of Reactions*, *Part I*, edited by C. F. Bernasconi, "Techniques of Chemistry, Vol. 6" (Wiley, New York, 1986), p. 565. (b) D. G. Truhlar, D.-h. Lu, S. C. Tucker, X. G. Zhao, A. Gonzàlez-Lafont, T. N. Truong, D. Maurice, Y-.P. Liu, and G. C. Lynch, in *Isotope Effects in Gas-Phase Chemsitry*, edited by J. A. Kaye (American Chemical Society Symposium Series 502, Washington, DC, 1992), p. 16.

[10]S. Baer, D. G. Fleming, D. Arseneau, M. Senba, and A. Gonzalez, in *Isotope Effects in Gas-Phase Chemistry*, edited by J. A. Kaye (American Chemical Society Symposium Series 502, Washington, DC, 1992), p. 111.

[11]J. J. Pan, D. J Arseneau, M. Senba, M. Shelly, and D. G. Fleming, J. Phys. Chem. A **101**, 8470 (1997)

[12]U. Himmer, H. Dilger, and E. Roduner, J. J. Pan, D. J Arseneau, and D. G. Fleming, M. Senba, J. Phys. Chem. A **103**, 2076 (1999).

[13](a) I. D. Reid, D. M. Garner, L. Y. Lee, M. Senba, D. J. Arsenneau, and D.G. Fleming, J. Chem. Phys. **121**, 80 (1989). (b) D. M. Garner, D. G. Fleming, and R. J. Mikula, Chem. Phys. Lett. **121**, 80 (1985).

[14]A. C. Gonzalez, I. D. Reid, D. M. Garner, M. Senba, D. G. Fleming, D. J. Arseneau, and J. R. Kempton, J. Chem. Phys. **91**, 6164 (1989).

[15]R. Snooks, D. J. Arseneau, D. G. Fleming, M. Senba, J. J. Pan, M. Shelley, and S. Baer, J. Chem. Phys. **102**, 4860 (1995).

[16]R. Snooks, D. J. Arsenau, S. Baer, D. G. Fleming, M. Senba, J. J. Pan, and M. Shelley, Hyperfine Interactions **87**, 991 (1994).

[17]J. V. Michael and G. N. Suess. J. Chem. Phys. **58**, 2807 (1973).

[18]J. A. Cowfer and J. V. Michael, J. Chem. Phys. **62**, 3504 (1975).

[19]B. C. Garrett, D. G. Truhar, and C. F. Melius, Phys. Rev. A **24**, 2853 (1981).

[20]N. C. Blais, D. G. Truhlar, and B. C. Garrett, J. Chem. Phys. **78**, 2363 (1983).

[21]D. McKenna and B. J. Webster, Chem. Soc. Faraday Trans. II **81**, 225 (1985).

[22]T. Takayanagi, K. M. Nakamura, M. Okamato, S. Sato, and G. C. Schatz, J. Chem. Phys. **86**, 6113 (1987).

[23](a) J. Villa, J. C. Corchado, A. Gonzalez-Lafont, J. M. Lluch, and D. G. Truhlar, J. Amer. Chem. Soc. **120**, 12141 (1998). (b) J. Villa, J. C. Corchado, A. Gonzalez-Lafont, J. M. Lluch, and D. G. Truhlar, J. Phys. Chem. A **103**, 5061 (1999).

[24]G. C. Lynch, D. G. Truhlar, F. B. Brown, and J.-g. Zhao, Hyperfine Interactions **87**, 885 (1994).

[25]D. G. Truhlar, in *The Reaction Path in Chemistry: Current Approaches and Perspectives*, edited by D. Heidrich (Kluwer, Dordrecht, 1995), p. 229.

[26]B. C. Garrett and D. G. Truhlar, J. Chem. Phys. **70**, 1593 (1979).

[27]D. G. Truhlar, A. D. Isaacson, R. T. Skodje, and B. C. Garrett, J. Phys. Chem. **86**, 2252 (1982).

[28]Y.-P. Liu, G. C. Lynch, T. N. Truong, D.-h. Lu, D. G. Truhlar, and B. C. Garrett, J. Am. Chem. Soc. **115**, 2408 (1993).

[29]D.-h. Lu, T. N. Truong, V. S. Melissas, G. C. Lynch, Y.-P. Liu, B. C. Garrett, R. Steckler, A. D. Isaacson, S. N. Rai, G. C. Hancock, J. G. Lauderdale, T. Joseph, and D. G. Truhlar, Computer Phys. Commun. **71**, 235 (1992).

[30]T. N. Truong, D.-h. Lu, G. C. Lynch, Y.-P. Liu, V. S. Melissas, J. J. P. Stewart, R. Steckler, B. C. Garrett, A. D. Isaacson, A. González-Lafont, S. N. Rai, G. C. Hancock, T. Joseph, and D. G. Truhlar, Computer Phys. Commun. **75**, 143 (1993).

[31]A. Fernandez-Ramos and D. G. Truhlar, J. Chem. Phys. **114**, 1491 (2001).

[32]Y.-P. Liu, D.-h. Lu, A. González-Lafont, D. G. Truhlar, and B. C. Garrett, J. Am. Chem. Soc. **115**, 7806 (1993).

[33]G. C. Schatz, H. F. Waquer, and T. H. Dunning, J. Phys. Chem. **88**, 221 (1984).

[34]B. J. Lynch and D. G. Truhlar, J. Phys. Chem. A **105**, 2936 (2001).

[35](a) A. Gonzàlez-Lafont, J. Villà, J. M. Lluch, J. Bertrán, R. Steckler, and D. G. Truhlar, J. Phys. Chem. A **102**, 3420 (1998). (b) P. L. Fast, J. C. Corchado, and D. G. Truhlar, J. Chem. Phys. **109**, 6237 (1998).

[36](a) C. F. Jackels, Z. Gu, and D. G. Truhlar, J. Chem. Phys. **102**, 3188 (1995). (b) Y.-Y. Chuang and D. G. Truhlar, J. Phys. Chem. A **102**, 232 (1998).

[37]D. G. Truhlar, A. D. Isaacson, and B. C. Garrett, in *Theory of Chemical Reaction Dynamics*, edited by M. Baer (CRC Press, Boca Raton, FL, 1985), p. 65.

[38]J. M. Rodgers, P. L. Fast, and D. G. Truhlar, J. Chem. Phys. **112**, 314 (2000).

[39]J. Pu, J. C. Corchado, B. J. Lynch, P. L. Fast, and D. G. Truhlar, MULTILEVELRATE–version 8.7, University of Minnesota, Minneapolis, 2001.

[40]Y. -Y. Chuang, J. Corchado, P. L. Fast, J. Villa, W. -P. Hu, Y. -P. Liu, G. C. Lynch, K. Nguyen, C. F. Jackels, M. Z. Gu, I. Rossi, S. Clayton, V. Melissas, B.J. Lynch, E. L. Coitiño, A. Fernandez-Ramos, J. Pu, R. Steckler, B. C. Garrett, A. D. Isaacson, and D. G. Truhlar, POLYRATE–version 8.7, University of Minnesota, Minneapolis, 2001.

[41]J. M. Rodgers, B. J. Lynch. P. L. Fast., Y -Y. Chuang, J. Pu, and D. G. Truhlar, MULTILEVEL–version 2.3, University of Minnesota, Minneapolis, 2001.

[42]J. C. Corchado, Y. -Y, Chuang, E. L. Coitiño, and D. G. Truhlar, GAUSSRATE-version 8.7, University of Minnesota, Minneapolis, 2001.

[43]GAUSSIAN98, by M. J. Frisch, G. W. Trucks, H. B. Schlegel, G. E. Scuseria, M. A. Robb, J. R. Cheeseman, V. G. Zakrzewski, J. A. Montgomery, R. E. Stratmann, J. C. Burant, S. Dapprich, J. M. Millam, A. D. Daniels, K. N. Kudin, M. C. Strain, O. Farkas, J. Tomasi, V. Barone, M. Cossi, R. Cammi, B. Mennucci, C. Pomelli, C. Adamo, S. Clifford, J. Ochterski, G. A. Petersson, P. Y. Ayala, Q. Cui, K. Morokuma, D. K. Malick, A. D. Rabuck, K. Raghavachari, J. B. Foresman, J. Cioslowski, J. V. Ortiz, B. B Stefanov, G. Liu, A. Liashenko, P. Piskorz, I. Komaromi, R. Gomperts, R. L. Martin, D. J. Fox, T. Keith, M. A. Al-Laham, C. Y. Peng, A. Nanayakkara, C. Gonzalez, M. Challacombe, P. M. W. Gill, B. G. Johnson, W. Chen, M. W. Wong, J. L. Andres, M. Head-Gordon, E.S. Replogle, and J. A. Pople, Gaussian, Inc., Pittsburgh, PA, 1998.

[44]G. Herzberg, *Spectra of Diatomic Molecules*, 2nd ed. (D. Van Nostrand, Princeton, 1950), p. 101.

[45](a) J. S. Shapiro and R. E. Weston, J. Phys. Chem. **76**, 1669 (1972). (b) A. E. Rodriguez, and P. D. Pacey, J. Phys. Chem. **90**, 6298 (1986). (c) P. C. Kobrinsky and P. D. Pacey, Can. J. Chem. **52**, 3665 (1972).

[46]J. Espinosa-García and J. C. Corchado, J. Phys. Chem. A **100**, 16561(1996).

[47](a) J. A. Kerr and M. J. Parsonage, *Evaluated Kinetic Data on Gas Phase Hydrogen Transfer Reactions of Methyl Radicals* (Butterworths, London, 1976). (b) N. L. Arthur and P. J. Newitt, Can. J. Chem. **63**, 3486 (1985). (c) W. Tsang and R. F. Hampson, J. Phys. Chem. Ref. Data **15**, 1087 (1986).

[48]M. J. Kurylo, G. A. Hollinden, and R. B. Timmons, J. Chem. Phys. **52**, 1773 (1970).

[49](a) R. C. Tolman, J. Am. Chem. Soc. **42**, 2506 (1920). (b) D. G. Truhlar, J. Chem. Educ. **55**, 309 (1978).

[50](a) D. G. Truhlar and J. C. Gray, Chem. Phys. Lett. **57**, 93 (1978). (b) N. C. Blais, D. G. Truhlar, and B. C. Garrett, J. Chem. Phys. **85**, 1094 (1981). (c) N. C. Blais, D. G.

Truhlar, and B. C. Garrett, J. Chem. Phys. **76**, 2768 (1982). (d) B. C. Garrett, D. G. Truhlar, J. M. Bowman, A. F. Wagner, D. Robie, S. Arepalli, N. Presser, and R. J. Gordon, J. Am. Chem. Soc. **108**, 3515 (1986).

[51]T. C. Allison and D. G. Truhlar, in *Modern Methods for Multidimensional Dynamics Computations in Chemistry*, edited by D. L. Thompson (World Scientific, Singapore, 1998), p. 618.

[52]J. Pu, J. C. Corchado, and D. G. Truhlar, J. Chem. Phys. **115**, 6266 (2001).

[53]J. M. L. Martin, J. Chem. Phys. **97**, 5012 (1992).

[54]*JANAF* Thermochemical Tables (U. S. Government Printing Office, Washington, DC, 1971), Vol. 37.

[55](a) D. K. Bondi, D.C. Clary, J. N. L Connor, B. C. Garrett, and D. G. Truhlar, J. Chem. Phys. **76**, 4986 (1982). (b) B. C. Garrett, R. Steckler, and D. G. Truhlar, Hyperfine Interactions **32**, 779 (1986).

[56]B. C. Garrett and D. G. Truhlar, J. Chem. Phys. **82**, 4543 (1985), **84**, 7057 (E) (1986).

[57]See, for example, R. D. Levine and R. B. Bernstein, *Molecular Reaction Dynamics and Chemical Reactivity* (Oxford University Press, New York, 1987), p.173.

[58](a) D. G. Truhlar and B. C. Garrett, J. Chim. Phys. **84**, 365 (1987). (b) D. G. Truhlar and M. S. Gordon, Science **249**, 491 (1990).

Table 1. Reactions considered in the present work.

Reaction	Symmetry number σ	Label	ΔH_0(kcal/mol)	
			MC-QCISD-SRP	MCG3-SRP
$CH_4 + H \rightarrow CH_3 + H_2$	4	R1	0.47	0.10[a]
$CH_3 + H_2 \rightarrow CH_4 + H_2$	4	R2	-0.47	-0.18
$CH_4 + D \rightarrow CH_3 + HD$	4	R3	-0.36	-0.65
$CH_3 + HD \rightarrow CH_4 + D$	2	R4	0.36	0.65
$CH_3 + DH \rightarrow CH_3D + H$	2	R5	-1.44	-1.18
$CH_4 + Mu \rightarrow CH_3 + H\text{-}Mu$	4	R6	8.00	7.45[a]
$CD_3 + H_2 \rightarrow CD_3H + H$	4	R7	-1.00	-0.83
$CD_3 + D_2 \rightarrow CD_4 + D$	4	R8	-1.12	-0.90
$CD_3 + HD \rightarrow CD_3H + D$	2	R9	-0.22	0.02
$CD_3 + DH \rightarrow CD_4 + H$	2	R10	-2.10	-1.90
$CH_3 + D_2 \rightarrow CH_3D + D$	4	R11	-0.46	-0.17

[a]The H-H (Mu) force constant is scaled for MCG3-SRP calculations on reactions R1 and R6, but not for the other cases.

Table 2. Kinetic isotope effects CH_3+H_2/CH_3+D_2

	MPW60					MC-QCISD-SRP					MCG3-SRP					Exp.[a]
T(K)	TST	CVT	CVT /SCT	CVT /LCT	CVT /μOMT	TST	CVT	CVT /SCT	CVT /LCT	CVT /μOMT	TST	CVT	CVT /SCT	CVT /LCT	CVT /μOMT	
400	3.14	2.68	5.04	3.98	5.04	2.91	2.39	4.13	3.49	4.13	3.22	2.70	4.58	3.73	4.57	4.8 ± 0.4[b]
500	2.80	2.50	3.67	3.11	3.67	2.60	2.26	3.14	2.80	3.14	2.83	2.49	3.43	2.96	3.43	3.5 ± 0.2[b]
600	2.54	2.34	3.02	2.68	3.02	2.37	2.14	2.66	2.45	2.66	2.54	2.31	2.86	2.57	2.86	2.8 ± 0.2[b]
829	2.14	2.04	2.31	2.16	2.31	2.02	1.91	2.11	2.02	2.11	2.12	2.01	2.22	2.09	2.22	2.4 ± 0.6[b]
930	2.02	2.20	2.13	2.02	2.13	1.91	1.83	1.97	1.90	1.97	2.00	1.91	2.06	1.96	2.06	2.1 ± 0.6[b]

[a]Ref. 45. Results below 667 K from Ref. 45a and results at 829 and 930 K calculated from 45b and 45c
[b]Values taken from Ref. 46

Table 3. Kinetic isotope effects CH_3+HD/CH_3+DH

	MPW60					MC-QCISD-SRP					MCG3-SRP					Exp.[a]
T(K)	TST	CVT	CVT /SCT	CVT /LCT	CVT /μOMT	TST	CVT	CVT /SCT	CVT /LCT	CVT /μOMT	TST	CVT	CVT /SCT	CVT /LCT	CVT /μOMT	
467	1.51	1.49	2.03	1.77	2.03	1.60	1.46	1.85	1.70	1.85	1.50	1.46	1.83	1.61	1.83	2.1 ± 0.5[b]
531	1.48	1.46	1.85	1.65	1.85	1.55	1.43	1.72	1.60	1.72	1.47	1.43	1.71	1.53	1.71	1.9 ± 0.3[b]
650	1.44	1.42	1.66	1.52	1.66	1.49	1.39	1.57	1.49	1.57	1.43	1.39	1.56	1.44	1.56	1.2 ± 0.3[b]

[a]Ref. 45a
[b]Values taken from Ref. 46

Table 4. Kinetic isotope effects CH_3+H_2/CD_3+H_2

	MPW60					MC-QCISD-SRP					MCG3-SRP					Exp.[a]
T(K)	TST	CVT	CVT /SCT	CVT /LCT	CVT /μOMT	TST	CVT	CVT /SCT	CVT /LCT	CVT /μOMT	TST	CVT	CVT /SCT	CVT /LCT	CVT /μOMT	
400	0.72	0.76	0.78	0.80	0.78	0.80	0.83	0.90	0.87	0.90	0.75	0.79	0.81	0.83	0.81	0.85[b]
500	0.81	0.84	0.85	0.86	0.85	0.87	0.89	0.94	0.92	0.94	0.83	0.86	0.88	0.88	0.88	0.86[b]
600	0.87	0.89	0.90	0.91	0.90	0.92	0.93	0.97	0.95	0.97	0.88	0.90	0.92	0.92	0.92	0.87[b]
700	0.90	0.92	0.93	0.94	0.93	0.94	0.95	0.98	0.97	0.98	0.92	0.93	0.95	0.95	0.95	0.88[b]

[a]Refs. 45a, 47
[b]Values taken from Ref. 9b

Table 5. Kinetic isotope effects CH_3+D_2/CD_3+D_2

	MPW60					MC-QCISD-SRP					MCG3-SRP					Exp.[a]
T(K)	TST	CVT	CVT /SCT	CVT /LCT	CVT /μOMT	TST	CVT	CVT /SCT	CVT /LCT	CVT /μOMT	TST	CVT	CVT /SCT	CVT /LCT	CVT /μOMT	
400	0.72	0.73	0.66	0.76	0.66	0.80	0.82	0.82	0.84	0.82	0.75	0.77	0.74	0.78	0.74	0.59[b]
500	0.81	0.82	0.76	0.84	0.76	0.87	0.88	0.89	0.90	0.89	0.83	0.84	0.82	0.85	0.82	0.72[b]
600	0.87	0.87	0.83	0.89	0.83	0.92	0.92	0.93	0.93	0.93	0.88	0.89	0.88	0.90	0.88	0.82[b]
700	0.90	0.91	0.88	0.92	0.88	0.94	0.95	0.96	0.96	0.96	0.92	0.92	0.91	0.93	0.91	0.90[b]

[a]Refs. 45a, 47
[b]Values taken from Ref. 9b

Table 6. Kinetic isotope effects CD_3+HD/CD_3+DH

	MPW60					MC-QCISD-SRP					MCG3-SRP					Exp.[a]
T(K)	TST	CVT	CVT /SCT	CVT /LCT	CVT /μOMT	TST	CVT	CVT /SCT	CVT /LCT	CVT /μOMT	TST	CVT	CVT /SCT	CVT /LCT	CVT /μOMT	
400	1.55	1.48	2.08	1.89	2.08	1.67	1.47	2.04	1.80	2.04	1.55	1.47	1.91	1.70	1.91	1.85
500	1.49	1.45	1.79	1.65	1.79	1.58	1.43	1.76	1.60	1.76	1.49	1.43	1.69	1.54	1.60	1.61
600	1.46	1.42	1.64	1.53	1.64	1.51	1.39	1.61	1.50	1.61	1.45	1.40	1.56	1.46	1.56	1.47
700	1.43	1.39	1.55	1.47	1.55	1.47	1.37	1.52	1.44	1.52	1.42	1.37	1.49	1.41	1.49	1.38

[a]Ref. 45a

Table 7. Kinetic isotope effects CD_3+H_2/CD_3+D_2

	MPW60					MC-QCISD-SRP					MCG3-SRP					Exp.[a]
T(K)	TST	CVT	CVT /SCT	CVT /LCT	CVT /μOMT	TST	CVT	CVT /SCT	CVT /LCT	CVT /μOMT	TST	CVT	CVT /SCT	CVT /LCT	CVT /μOMT	
400	3.14	2.47	4.26	3.76	4.26	2.91	2.35	3.79	3.34	3.79	3.22	2.62	4.14	3.50	4.13	3.33
500	2.80	2.44	3.30	3.01	3.30	2.61	2.23	2.98	2.73	2.98	2.83	2.44	3.22	2.85	3.21	2.88
600	2.54	2.30	2.80	2.62	2.80	2.37	2.12	2.56	2.41	2.56	2.54	2.28	2.73	2.51	2.73	2.61
700	2.34	2.17	2.49	2.37	2.49	2.19	2.01	2.30	2.20	2.30	2.33	2.14	2.43	2.27	2.43	2.43

[a]Ref. 45a

Table 8. Kinetic isotope effects CH_4+H/CH_4+D

	MPW60					MC-QCISD-SRP					MCG3-SRP					Exp.[a]
T(K)	TST	CVT	CVT /SCT	CVT /LCT	CVT /μOMT	TST	CVT	CVT /SCT	CVT /LCT	CVT /μOMT	TST	CVT	CVT /SCT	CVT /LCT	CVT /μOMT	
400	0.51	0.47	0.55	0.51	0.55	0.51	0.49	0.60	0.54	0.60	0.54	0.50	0.58	0.54	0.58	0.74
500	0.62	0.59	0.64	0.62	0.64	0.62	0.61	0.68	0.64	0.68	0.65	0.62	0.67	0.65	0.67	0.84
600	0.70	0.68	0.71	0.70	0.71	0.70	0.70	0.75	0.72	0.75	0.73	0.70	0.74	0.73	0.74	0.91
700	0.76	0.74	0.77	0.76	0.77	0.76	0.76	0.80	0.78	0.80	0.78	0.77	0.79	0.79	0.79	0.97

[a]Ref. 48

Table 9. Kinetic isotope effects CH_3+H_2/CD_3+D_2

	MPW60					MC-QCISD-SRP					MCG3-SRP					Exp.[a]
T(K)	TST	CVT	CVT /SCT	CVT /LCT	CVT /μOMT	TST	CVT	CVT /SCT	CVT /LCT	CVT /μOMT	TST	CVT	CVT /SCT	CVT /LCT	CVT /μOMT	
400	2.26	1.96	3.32	3.01	3.32	2.33	1.95	3.37	2.89	3.37	2.42	2.06	3.37	2.89	3.37	2.82, 2.83
500	2.27	2.04	2.81	2.60	2.81	2.27	1.99	2.80	2.51	2.80	2.36	2.10	2.82	2.52	2.82	2.52, 2.48
600	2.20	2.04	2.52	2.37	2.52	2.18	1.97	2.47	2.29	2.47	2.06	2.06	2.51	2.31	2.51	2.30, 2.27

[a]First value is Table 2 × Table 5; second value is Table 4 × Table 7

Table 10. Reaction rate constants ($cm^3molecule^{-1}s^{-1}$) for CH_4 + Mu

		MPW60					MC-QCISD-SRP					MCG3-SRP					Exp.[b]
T(K)	Power of ten[a]	TST	CVT	CVT /SCT	CVT /LCT	CVT /μOMT	TST	CVT	CVT /SCT	CVT /LCT	CVT /μOMT	TST	CVT	CVT /SCT	CVT /LCT	CVT /μOMT	
626	-17	6.5	2.9	4.1	4.3	4.3	7.6	3.9	4.7	5.2	5.2	11.7	5.2	7.1	7.5	7.5	19.0[c]
634	-17	8.1	3.7	5.1	5.4	5.4	9.4	4.9	5.8	6.4	6.4	14.3	6.5	8.8	9.3	9.3	20.8
662	-16	1.6	7.7	1.0	1.1	1.1	1.9	1.0	1.2	1.3	1.3	2.8	1.3	1.8	1.8	1.8	3.7
668	-16	1.9	1.0	1.2	1.2	1.2	2.2	1.2	1.4	1.5	1.5	3.2	1.6	2.0	2.1	2.1	4.8
691	-16	3.1	1.6	2.0	2.1	2.1	3.7	2.0	2.3	2.5	2.5	5.4	2.7	3.4	3.5	3.5	8.6
721	-16	5.9	3.1	3.9	4.0	4.0	6.9	3.9	4.4	4.8	4.8	9.9	5.2	6.3	6.6	6.6	17.4
732	-16	7.3	3.9	4.8	5.0	5.0	8.7	5.0	5.5	6.0	6.0	12.3	6.5	7.9	8.2	8.2	22.6
776	-15	1.6	0.9	1.1	1.1	1.1	2.0	1.2	1.3	1.4	1.4	2.7	1.5	1.8	1.8	1.8	6.7
821	-15	3.5	2.0	2.3	2.4	2.4	4.2	2.6	2.8	2.9	2.9	5.6	3.3	3.7	3.9	3.9	16.0

[a]All values in a given row are to be multiplied by 10 to this power

[b]Ref. 15

[c]The experimental error bar (Ref. 15) is 30% for the two lowest temperatures and smaller for other temperatures

Table 11. Reaction rate constants ($cm^3molecule^{-1}s^{-1}$) for CH_4 + H

		MPW60					MC-QCISD-SRP					MCG3-SRP					Exp.	
T(K)	Power of ten[a]	TST	CVT	CVT /SCT	CVT /LCT	CVT /μOMT	TST	CVT	CVT /SCT	CVT /LCT	CVT /μOMT	TST	CVT	CVT /SCT	CVT /LCT	CVT /μOMT	*b*	*c*
626	-15	2.4	2.2	3.6	3.0	3.6	2.7	2.4	3.9	3.2	3.9	3.1	2.8	4.4	3.7	4.4	4.0	4.0
634	-15	2.7	2.5	4.1	3.4	4.1	3.1	2.7	4.4	3.7	4.4	3.5	3.2	5.0	4.2	5.0	4.5	4.6
662	-15	4.4	4.1	6.4	5.4	6.4	5.1	4.5	7.0	5.9	7.0	5.7	5.2	7.9	6.7	7.9	7.0	7.3
668	-15	4.9	4.5	7.0	5.9	7.0	5.6	5.0	7.7	6.5	7.7	6.3	5.8	8.6	7.4	8.6	7.6	8.0
691	-15	7.0	6.5	9.8	8.4	9.8	8.1	7.3	10.9	9.3	10.9	9.1	8.3	12.1	10.4	12.1	10.6	11.2
721	-14	1.1	1.0	1.5	1.3	1.5	1.3	1.2	1.7	1.4	1.7	1.4	1.3	1.8	1.6	1.8	1.6	1.7
732	-14	1.1	1.2	1.7	1.5	1.7	1.5	1.4	1.9	1.7	1.9	1.7	1.5	2.1	1.9	2.1	1.8	2.0
776	-14	2.3	2.1	2.9	2.6	2.9	2.7	2.5	3.4	3.0	3.4	2.9	2.7	3.6	3.2	3.6	3.1	3.6
821	-14	3.9	3.7	4.8	4.3	4.8	4.6	4.3	5.6	5.0	5.6	5.0	4.7	6.0	5.4	6.0	5.0	5.9

[a]All values in a given row are to be multiplied by 10 to this power. Note that the results in this table and in the subsequent tables involving H + CH_4 are for the same potential energy surface parameters we used for this reaction in Ref. 1.

[b]Ref. 8a: experimental

[c]Ref. 8b: experimental at 776 – 821 K and extrapolated at 626 – 776 K.

Table 12. Kinetic isotope effects CH_4+Mu/CH_4+H

	MPW60					MC-QCISD-SRP					MCG3-SRP					Exp.	
T(K)	TST	CVT	CVT /SCT	CVT /LCT	CVT /μOMT	TST	CVT	CVT /SCT	CVT /LCT	CVT /μOMT	TST	CVT	CVT /SCT	CVT /LCT	CVT /μOMT	*a*	*b*
626	0.028	0.014	0.012	0.015	0.012	0.028	0.016	0.012	0.016	0.014	0.038	0.019	0.016	0.021	0.017	0.048	0.047
634	0.030	0.015	0.012	0.016	0.013	0.030	0.018	0.013	0.018	0.015	0.040	0.020	0.017	0.022	0.018	0.046	0.045
662	0.037	0.019	0.016	0.020	0.017	0.037	0.022	0.017	0.022	0.019	0.049	0.026	0.022	0.028	0.023	0.053	0.051
668	0.038	0.020	0.017	0.021	0.018	0.039	0.023	0.018	0.023	0.019	0.051	0.027	0.023	0.029	0.025	0.063	0.060
691	0.045	0.024	0.021	0.025	0.022	0.045	0.028	0.021	0.027	0.023	0.059	0.032	0.028	0.034	0.029	0.082	0.077
721	0.054	0.030	0.026	0.031	0.027	0.054	0.034	0.027	0.033	0.029	0.070	0.039	0.035	0.041	0.036	0.111	0.103
732	0.057	0.032	0.028	0.034	0.029	0.058	0.036	0.029	0.036	0.031	0.074	0.042	0.037	0.044	0.039	0.125	0.116
776	0.073	0.043	0.038	0.044	0.039	0.073	0.047	0.038	0.046	0.041	0.091	0.055	0.049	0.057	0.050	0.220	0.185
821	0.090	0.055	0.049	0.056	0.050	0.090	0.060	0.049	0.058	0.052	0.112	0.070	0.062	0.071	0.064	0.320	0.272

[a]Experimental rate constants in Table 10 divided by experimental rate constants of Ref. 8a in Table 11
[b]Experimental rate constants in Table 10 divided by experimental (T = 776 – 821 K) and extrapolated (626 – 732 K) rate constants of Ref. 8b in Table 11.

Table 13. Arrhenius activation energies (kcal/mol) at 650 K[a]

	MPW60			MCG3-SRP			Exp.
Reaction	TST	CVT	CVT/μOMT	TST	CVT	CVT/μOMT	
$CH_4 + H$	14.4	14.6	13.3	14.4	14.6	13.4	12.8[b]
$CH_4 + D$	13.7	13.8	12.6	13.7	13.8	12.8	12.3[c]
$CH_4 + Mu$	20.7	22.1	20.9	20.1	21.6	20.4	20.6,[d] 24.6[e]
$CH_3 + H_2$	12.6	12.8	11.4	12.8	13.0	11.8	11.4[f]
$CD_3 + H_2$	12.2	12.0	11.1	12.5	12.7	11.5	11.3[g]
$CD_3 + D_2$	12.9	12.9	12.2	13.2	13.3	12.5	11.9[h]

[a]For theory, values are obtained by finite differentiation at 640 K and 660 K

[b]Analytic differentiation of experimental fit of k_1 (Ref. 8a) at 650 K

[c]Finite differentiation of experimental rate constants k_3 at 600 K and 700 K; experimental k_3 are from k_1 of Ref. 8 and experimental KIEs in Table 8

[d]Finite differentiation of experimental k_6 (Ref. 15) at 634 K and 668 K

[e]E_a of experimental Arrhenius fit of k_6 (Ref. 15). The values in the table are reduced to 20.0 kcal/mol (finite differentiation) and 23.3 kcal/mol (Ref. 15) if one shifts the high-temperature data as discuss in the text.

[f]Finite differentiation of the experimental rate constants k_2 at 640 K and 660 K; experimental k_2 are from k_1 of Ref. 8 and equilibrium constant of R1 and R2 (also Ref. 8)

[g]Finite differentiation of experimental rate constants k_7 at 600 K and 700 K; experimental k_7 are from k_2 explained in footnote *f* and experimental KIEs in Table 4

[h]Finite differentiation of experimental rate constants k_8 at 600 K and 700 K; experimental k_8 are from k_2 explained in footnote *f* and experimental KIEs in Table 9

Table 14. TST and CVT bottleneck properties for isotopic reactions on the MPW60 and MCG3-SRP surface[a]

Reaction CH_4 + Y	T(K)	MPW60							MCG3-SRP						
		s	$r_{C\text{-}H}$	$r_{H\text{-}Y}$	$V_{MEP}(s)$	ZPE(s)	V_a^G	ΔV_a^G	s	$r_{C\text{-}H}$	$r_{H\text{-}Y}$	$V_{MEP}(s)$	ZPE(s)	V_a^G	ΔV_a^G
CH_4+Mu															
	S.P.[b]	0.000	1.39	0.89	14.8	35.0	49.8	20.5	0.000	1.40	0.90	14.8	33.1	47.9	19.8
	0[c]	0.151	1.49	0.83	14.0	37.1	51.1	21.7	0.159	1.52	0.84	14.0	35.2	49.2	21.1
	600[c]	0.132	1.48	0.83	14.2	36.8	51.0	21.7	0.140	1.50	0.84	14.2	35.0	49.2	21.1
	1000[c]	0.108	1.46	0.84	14.4	36.4	50.9	21.6	0.112	1.47	0.84	14.5	34.6	49.0	20.9
CH_4+H															
	S.P.[b]	0.000	1.39	0.89	14.8	27.9	42.7	13.4	0.000	1.40	0.90	14.8	26.5	41.3	13.2
	0[c]	0.060	1.44	0.84	14.5	28.3	42.9	13.6	0.065	1.46	0.85	14.5	27.0	41.5	13.4
	600[c]	0.044	1.43	0.85	14.6	28.2	42.9	13.6	0.049	1.44	0.86	14.7	26.8	41.5	13.4
	1000[c]	0.032	1.42	0.86	14.7	28.1	42.8	13.5	0.038	1.43	0.87	14.7	26.8	41.5	13.4
CH_4+D															
	S.P.[b]	0.000	1.39	0.89	14.8	27.0	41.8	12.5	0.000	1.40	0.90	14.8	25.6	40.5	12.3
	0[c]	0.063	1.45	0.84	14.5	27.4	41.9	12.6	0.068	1.46	0.85	14.5	26.1	40.6	12.5
	600[c]	0.044	1.43	0.85	14.6	27.2	41.9	12.6	0.052	1.45	0.86	14.6	26.0	40.6	12.5
	1000[c]	0.038	1.42	0.86	14.7	27.2	41.9	12.6	0.047	1.44	0.86	14.6	25.9	40.6	12.6

[a]Distances in Å, energies in kcal/mol; note that ΔV_a^G is the difference between V_a^G at a given point along the reaction path and V_a^G at the reactant

[b]S. P. denotes saddle point

[c]CVT transition state at this T

Table 15. Zero point energy (ZPE) in the unscaled harmonic oscillator (HO) approximation and with

scaled force constants (SFC) for the making bond

Species	MPW60			MCG3-SRP		
	ZPE_{HO}	ZPE_{SFC}	$ZPE_{HO}-ZPE_{SFC}$	ZPE_{HO}	ZPE_{SFC}	$ZPE_{HO}-ZPE_{SFC}$
CH_4	29.3	29.3	0.0	28.1	28.1	0.0
CH_3	19.5	19.5	0.0	18.7	18.7	0.0
CH_5 (S. P.[a])	27.9	27.8	0.1	26.5	26.4	0.1
H_2	6.6	6.2	0.4	6.3	6.2	0.1
CH_4Mu (S. P.)	35.0	34.1	0.9	33.1	32.9	0.2
HMu	14.6	12.8	1.8	14.0	13.6	0.4

[a]S.P. denotes saddle point

Table 16. Reaction rate constants ($cm^3molecule^{-1}s^{-1}$) and KIEs for CH_4 + Mu and CH_4 + H on the MPW60 surface when the Mu-H stretching force constant is scaled by 0.7765 and the H-H stretching force constant is scaled by 0.8957

	CH_4 + Mu					CH_4 + H					KIE (k_{Mu} / k_H)					Exp.	
T(K)	TST	CVT	CVT /SCT	CVT /LCT	CVT /μOMT	TST	CVT	CVT /SCT	CVT /LCT	CVT /μOMT	TST	CVT	CVT /SCT	CVT /LCT	CVT /μOMT	*a*	*b*
400	1.9(-20)	6.7(-21)	1.8(-20)	2.1(-20)	2.1(-20)	5.2(-18)	4.8(-18)	1.9(-17)	1.2(-17)	1.9(-17)	0.004	0.001	0.001	0.002	0.001	n.a.[c]	n.a.
500	2.5(-18)	1.1(-18)	2.1(-18)	2.3(-18)	2.3(-18)	1.6(-16)	1.5(-16)	3.4(-16)	2.5(-16)	3.4(-16)	0.016	0.008	0.006	0.009	0.007	n.a.	n.a.
600	6.7(-17)	3.6(-17)	5.3(-17)	5.7(-17)	5.7(-17)	1.6(-15)	1.6(-15)	2.7(-15)	2.2(-15)	2.7(-15)	0.041	0.023	0.019	0.026	0.021	n.a.	n.a.
626	1.3(-16)	7.5(-17)	1.1(-16)	1.1(-16)	1.1(-16)	2.7(-15)	2.6(-15)	4.3(-15)	3.5(-15)	4.3(-15)	0.050	0.029	0.025	0.032	0.026	0.048	0.047
634	1.6(-16)	9.3(-16)	1.3(-16)	1.4(-16)	1.4(-16)	3.1(-15)	3.0(-15)	4.9(-15)	4.0(-15)	4.9(-15)	0.053	0.031	0.027	0.034	0.028	0.046	0.045
662	3.2(-16)	1.9(-16)	2.5(-16)	2.6(-16)	2.6(-16)	4.9(-15)	4.8(-15)	7.6(-15)	6.3(-15)	7.6(-15)	0.064	0.039	0.033	0.042	0.035	0.053	0.051
668	3.6(-16)	2.1(-16)	2.9(-16)	3.0(-16)	3.0(-16)	5.5(-15)	5.3(-15)	8.3(-15)	6.9(-15)	8.3(-15)	0.067	0.041	0.035	0.044	0.037	0.063	0.060
691	6.0(-16)	3.6(-16)	4.7(-16)	5.0(-16)	5.0(-16)	7.8(-15)	7.6(-15)	1.2(-14)	9.7(-15)	1.2(-14)	0.076	0.048	0.041	0.051	0.043	0.082	0.077
721	1.1(-15)	6.8(-16)	8.7(-16)	9.1(-16)	9.1(-16)	1.2(-14)	1.2(-14)	1.7(-14)	1.5(-14)	1.7(-14)	0.090	0.058	0.050	0.061	0.053	0.111	0.103
732	1.3(-15)	8.5(-16)	1.1(-15)	1.1(-15)	1.1(-15)	1.4(-14)	1.4(-14)	2.0(-14)	1.7(-14)	2.0(-14)	0.095	0.062	0.054	0.065	0.056	0.125	0.116
776	2.9(-15)	1.9(-15)	2.4(-15)	2.4(-15)	2.4(-15)	2.5(-14)	2.4(-14)	3.4(-14)	3.0(-14)	3.4(-14)	0.117	0.078	0.070	0.082	0.072	0.220	0.185
821	6.0(-15)	4.1(-15)	4.8(-15)	5.0(-15)	5.0(-15)	4.3(-14)	4.2(-14)	5.5(-14)	4.9(-14)	5.5(-14)	0.141	0.098	0.087	0.102	0.090	0.320	0.272

[a]Experimental rate constants in Table 10 divided by experimental rate constants of Ref. 8a in Table 11

[b]Experimental rate constants in Table 10 divided by experimental (T = 776 – 821 K) and extrapolated (T = 626 – 732 K) rate constants of Ref. 8b in Table 11.

[c]n.a. denotes not available

Table 17. Reaction rate constants ($cm^3molecule^{-1}s^{-1}$) and KIEs for CH_4 + Mu and CH_4 + H on the MCG3-SRP surface when the Mu-H stretching force constant is scaled by 0.9441 and the H-H stretching force constant is scaled by 0.9746

	CH_4 + Mu					CH_4 + H					KIE (k_{Mu} / k_H)					Exp.[a]
T(K)	TST	CVT	CVT /SCT	CVT /LCT	CVT /μOMT	TST	CVT	CVT /SCT	CVT /LCT	CVT /μOMT	TST	CVT	CVT /SCT	CVT /LCT	CVT /μOMT	
400	1.8(-20)	4.7(-21)	1.2(-20)	1.4(-20)	1.4(-20)	6.1(-18)	5.1(-18)	1.8(-17)	1.2(-17)	1.8(-17)	0.003	0.001	0.001	0.001	0.001	n.a.[b]
500	2.5(-18)	9.1(-19)	1.5(-18)	1.7(-18)	1.7(-18)	1.9(-16)	1.6(-16)	3.5(-16)	2.6(-16)	3.5(-16)	0.014	0.006	0.004	0.006	0.005	n.a.
600	6.9(-17)	3.1(-17)	4.4(-17)	4.7(-17)	4.7(-17)	1.9(-15)	1.7(-15)	2.9(-15)	2.4(-15)	2.9(-15)	0.036	0.018	0.015	0.020	0.016	n.a.
626	1.4(-16)	6.5(-17)	8.9(-17)	9.4(-17)	9.4(-17)	3.2(-15)	2.9(-15)	4.6(-15)	3.8(-15)	4.6(-15)	0.044	0.023	0.019	0.025	0.021	0.048
634	1.7(-16)	8.1(-17)	1.1(-16)	1.2(-16)	1.2(-16)	3.6(-15)	3.3(-15)	5.2(-15)	4.4(-15)	5.2(-15)	0.046	0.024	0.021	0.026	0.022	0.046
662	3.3(-16)	1.6(-16)	2.1(-16)	2.3(-16)	2.3(-16)	5.9(-15)	5.4(-15)	8.2(-15)	7.0(-15)	8.2(-15)	0.056	0.030	0.026	0.033	0.028	0.053
668	3.8(-16)	1.9(-16)	2.5(-16)	2.6(-16)	2.6(-16)	6.5(-15)	6.0(-15)	9.0(-15)	7.6(-15)	9.0(-16)	0.058	0.032	0.027	0.034	0.029	0.063
691	6.2(-16)	3.3(-16)	4.1(-16)	4.3(-16)	4.3(-16)	9.3(-15)	8.6(-15)	1.3(-15)	1.1(-14)	1.3(-14)	0.067	0.038	0.033	0.040	0.034	0.082
721	1.1(-15)	6.2(-16)	7.6(-16)	8.0(-16)	8.0(-16)	1.5(-14)	1.4(-14)	1.9(-14)	1.7(-14)	1.9(-14)	0.079	0.046	0.040	0.048	0.042	0.111
732	1.4(-15)	7.8(-16)	9.5(-16)	9.9(-16)	9.9(-16)	1.7(-14)	1.6(-14)	2.2(-14)	1.9(-14)	2.2(-14)	0.083	0.049	0.043	0.051	0.045	0.125
776	3.1(-15)	1.8(-15)	2.1(-15)	2.2(-15)	2.2(-15)	3.0(-14)	2.8(-14)	3.8(-14)	3.4(-14)	3.8(-14)	0.103	0.064	0.056	0.065	0.058	0.220
821	6.4(-15)	3.8(-15)	4.3(-15)	4.5(-15)	4.5(-15)	5.1(-14)	4.8(-14)	6.2(-14)	5.6(-14)	6.2(-14)	0.124	0.079	0.070	0.080	0.072	0.320

[a]Experimental rate constants in Table 9 divided by experimental rate constants in Table 10

[b]n.a. denotes not available

Table 18. Geometries of CH_3 on three SRP surfaces[a]

	MPW60	MC-QCISD-SRP	MCG3-SRP	Exp.[b]
C-H	1.072	1.080	1.080	1.079
∠H-C-H	120.0	120.0	120.0	120.0

[a]Distances in Å, angles in degrees
[b]Ref. 54

Table 19. Absolute rate constants (in $cm^3molecule^{-1}s^{-1}$) at 600 K and 700 K for all isotopic reactions in Table 1

			MPW60					MC-QCISD-SRP					MCG3-SRP				
Reaction	*T*(K)	Power of ten[a]	TST	CVT	CVT /SCT	CVT /LCT	CVT /μOMT	TST	CVT	CVT /SCT	CVT /LCT	CVT /μOMT	TST	CVT	CVT /SCT	CVT /LCT	CVT /μOMT
R1	600	-15	1.4	1.3	2.3	1.9	2.3	1.6	1.4	2.2	2.0	2.4	1.9	1.7	2.8	2.3	2.8
	700	-15	8.0	7.5	11.1	9.5	11.1	9.4	8.5	12.4	10.6	12.4	10.4	9.6	13.7	11.9	13.7
R2	600	-16	1.5	1.4	2.4	2.0	2.4	2.0	1.7	2.9	2.4	2.9	1.7	1.6	2.6	2.1	2.6
	700	-16	6.8	6.4	9.4	8.1	9.4	9.1	8.2	12.1	10.4	12.1	8.0	7.3	10.6	9.1	10.6
R3	600	-15	2.0	1.9	3.2	2.6	3.2	2.3	2.0	3.2	2.7	3.2	2.6	2.4	3.8	3.1	3.8
	700	-14	1.1	1.0	1.4	1.3	1.4	1.2	1.1	1.6	1.4	1.6	1.3	1.2	1.7	1.5	1.7
R4	600	-17	6.0	5.6	9.3	7.7	9.3	8.0	7.1	11.3	9.5	11.3	6.8	6.3	9.9	8.3	9.9
	700	-16	2.7	2.6	3.8	3.3	3.8	3.8	3.4	4.8	4.2	4.8	3.2	3.0	4.2	3.7	4.2
R5	600	-17	4.1	3.9	5.4	4.9	5.4	5.3	5.0	7.0	6.2	7.0	4.7	4.5	6.2	5.6	6.2
	700	-16	1.9	1.9	2.3	2.2	2.3	2.6	2.5	3.2	2.9	3.2	2.3	2.2	2.7	2.6	2.7
R6	600	-17	3.2	1.4	2.0	2.1	2.1	3.7	1.8	2.3	2.5	2.5	5.8	2.5	3.5	3.7	3.7
	700	-16	3.8	1.9	2.5	2.6	2.6	4.5	2.5	2.8	3.1	3.1	6.5	3.3	4.1	4.3	4.3
R7	600	-16	1.8	1.6	2.7	2.2	2.7	2.1	1.8	3.0	2.5	3.0	2.0	1.7	2.8	2.3	2.8
	700	-16	7.5	1.9	10.1	8.7	10.1	9.7	8.6	12.3	10.7	12.3	8.7	7.9	11.2	9.7	11.2
R8	600	-17	6.9	6.8	9.5	8.2	9.5	9.0	8.6	11.8	10.3	11.8	7.7	7.5	10.3	9.2	10.3
	700	-16	3.2	3.2	4.1	3.7	4.1	4.4	4.3	5.4	4.9	5.4	3.7	3.7	4.6	4.3	4.6
R9	600	-17	6.9	6.3	10.1	8.4	10.1	8.8	7.6	11.8	9.9	11.8	7.7	6.9	10.4	9.0	10.4
	700	-16	3.0	2.8	4.0	3.5	4.0	4.1	3.6	5.0	4.3	5.0	3.5	3.2	4.3	3.9	4.3
R10	600	-17	4.7	4.5	6.2	5.5	6.2	5.8	5.4	7.2	6.6	7.3	5.3	5.0	6.7	6.2	6.7
	700	-16	2.1	2.0	2.6	2.4	2.6	2.8	2.6	3.3	3.0	3.3	2.5	2.3	2.9	2.7	2.9

[a]All values in a given row are to be multiplied by 10 to this power

Figure Captions

Figure 1 Arrhenius plot for reaction R1 and R6 showing the experimental data and the MCG3-SRP results with scaled H-H and H-Mu force constants.

Figure 2 Ground-state vibrationally adiabatic potential curves for reactions R1 and R6 as obtained with the MCG3-SRP potential energy surface and scaled H-H and H-Mu force constants. For reaction R1 the curve is plotted for a scaling mass of 1 amu. For reaction R6 it is plotted for a scaling mass of 1 amu and also for a scaling mass equal to the mass of Mu.

Figure 3 Generalized normal mode frequencies as functions of reaction coordinate for MCG3-SRP calculations with scaled H-H and H-Mu force constants. (a) $H + CH_4 \rightarrow H_2 + CH_3$ (b) $Mu + CH_4 \rightarrow MuH + CH_3$. The reaction coordinate is scaled to 1 amu for (a) and to the mass of Mu for (b).

Figure 1

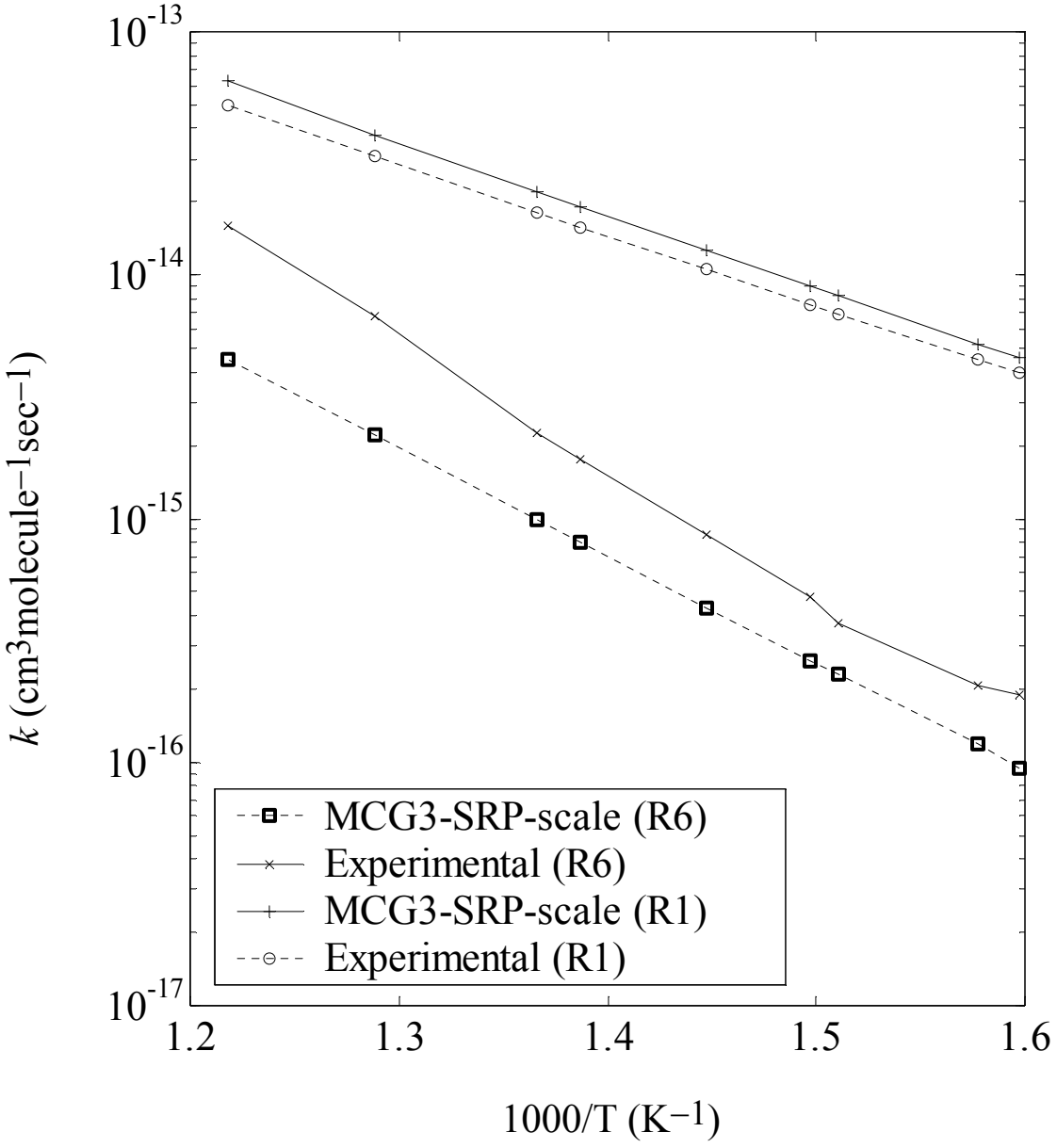
10-13
10-14
10-15
10-16
10-17
k (cm3molecule−1sec−1)
1.2
1.3
1.4
1.5
1.6
1000/T (K−1)
MCG3-SRP-scale (R6)
Experimental (R6)
MCG3-SRP-scale (R1)
Experimental (R1)

Figure 2

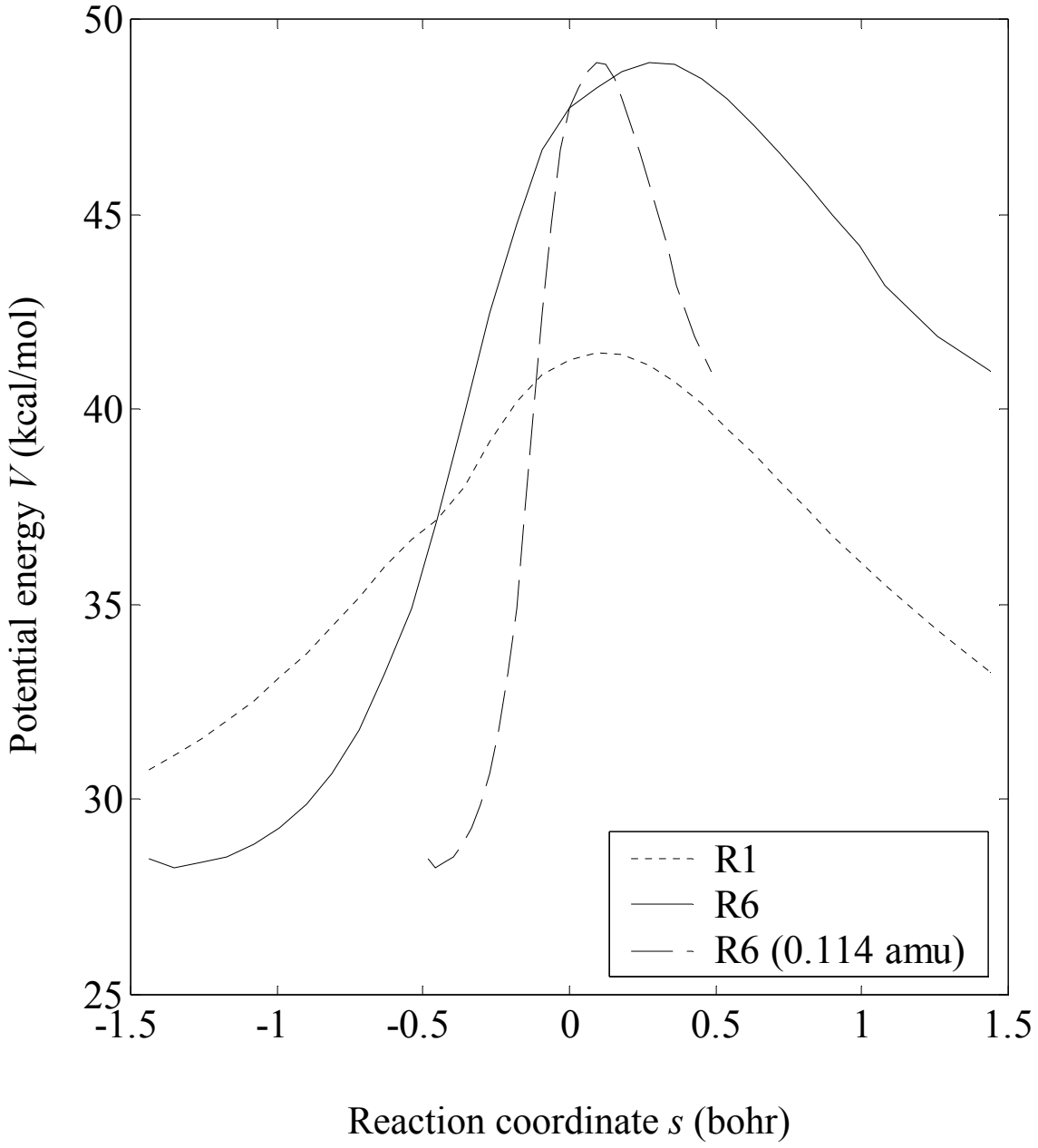
50
45
40
35
30
25
-1.5
-1
-0.5
0
0.5
1
1.5
Potential energy V (kcal/mol)
Reaction coordinate s (bohr)
R1
R6
R6 (0.114 amu)

Figure 3a

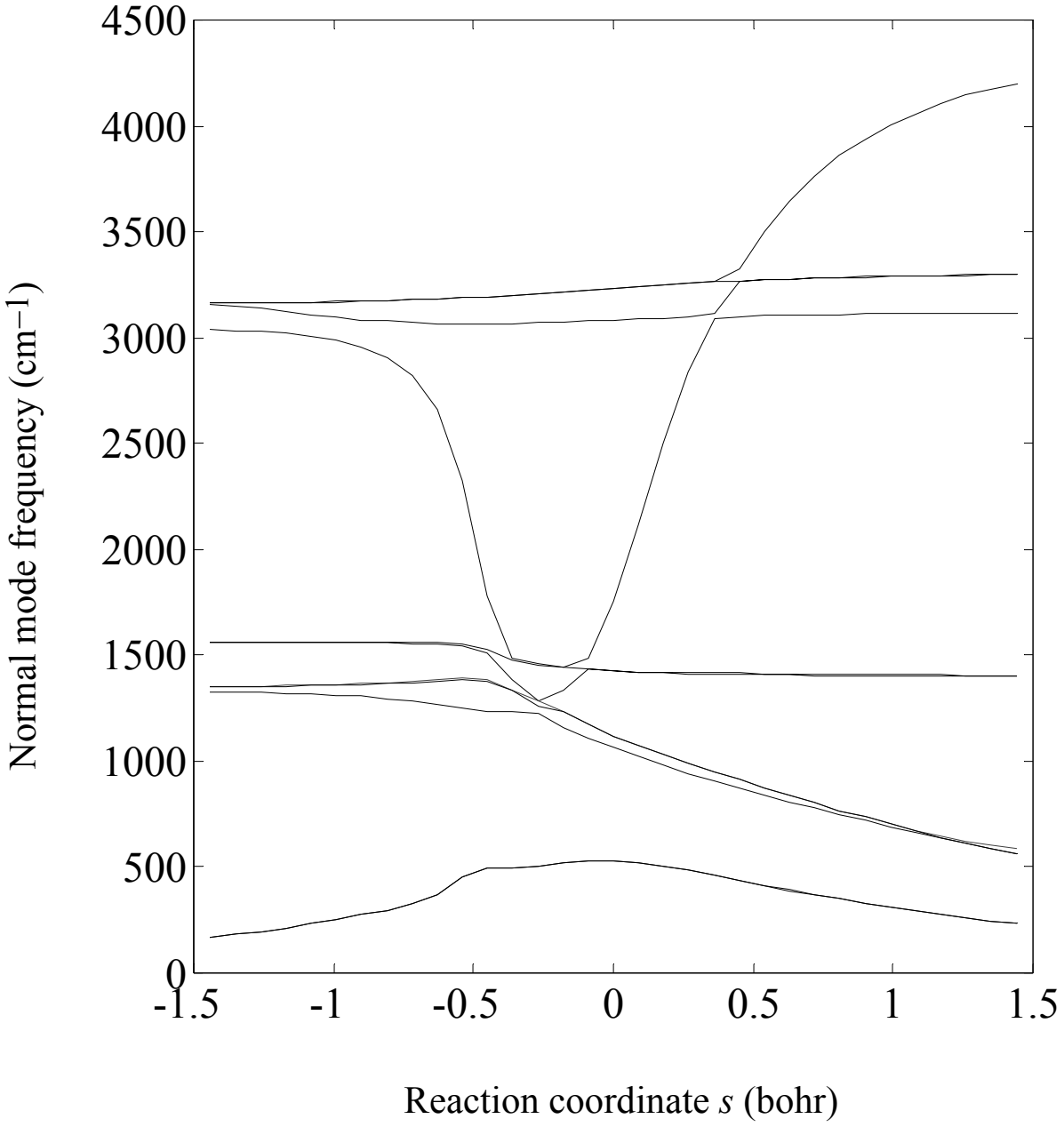
4500
4000
3500
3000
2500
2000
1500
1000
500
0
-1.5
-1
-0.5
0
0.5
1
1.5
Normal mode frequency (cm−1)
Reaction coordinate s (bohr)

Figure 3b

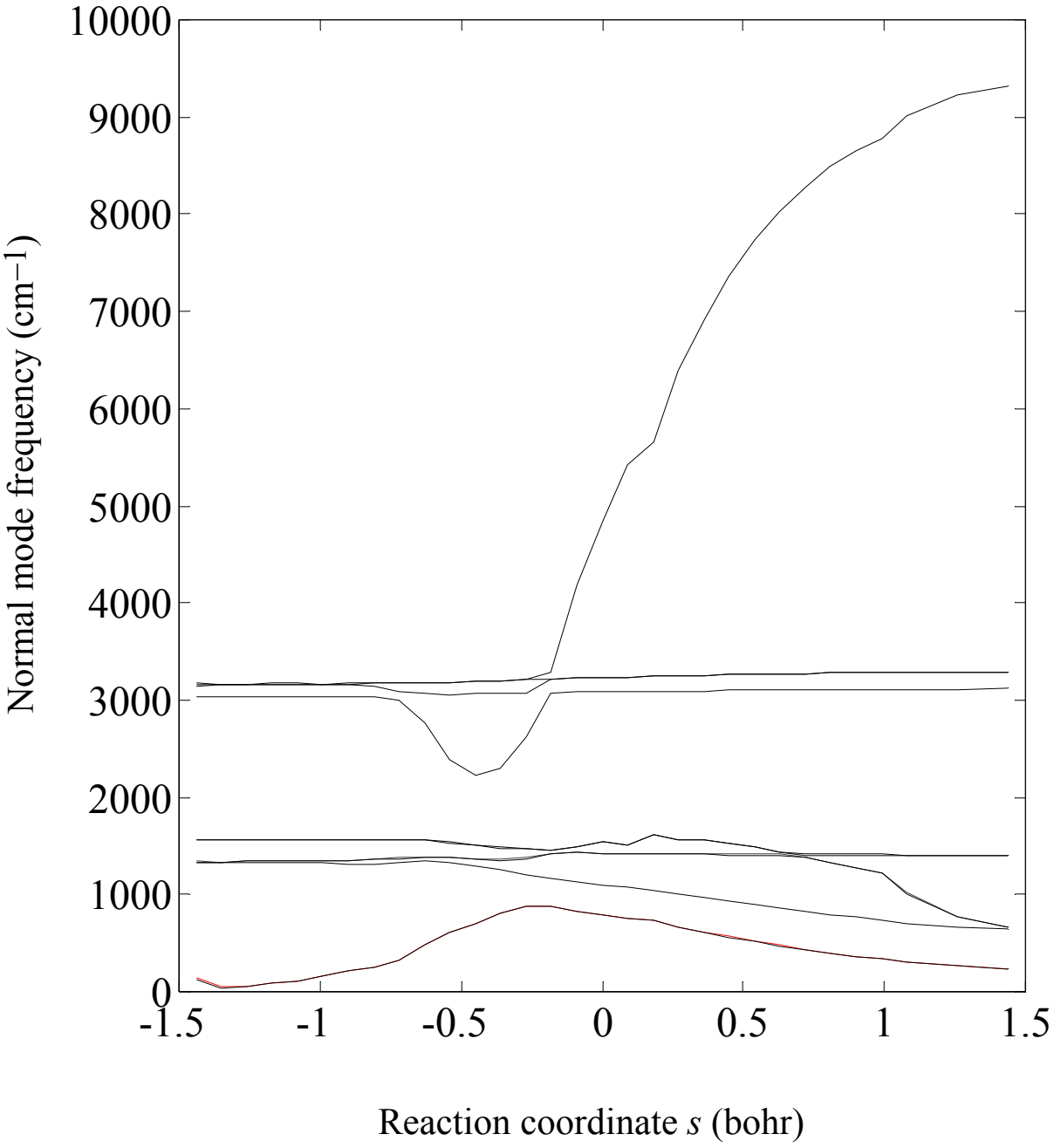
10000
9000
8000
7000
6000
5000
4000
3000
2000
1000
0
Normal mode frequency (cm−1)
-1.5
-1
-0.5
0
0.5
1
1.5
Reaction coordinate s (bohr)